Published in the Nuclear Instruments and Methods 122, 575 - 585 (1974)

LBL-3811
c.1

A BREMSSTRAHLUNG-IDENTIFICATION TECHNIQUE FOR COSMIC-RAY ELECTRONS AND POSITRONS

Andrew Buffington, Charles D. Orth, and George F. Smoot

September 19, 1974

Prepared for the U. S. Atomic Energy Commission
under Contract W-7405-ENG-48

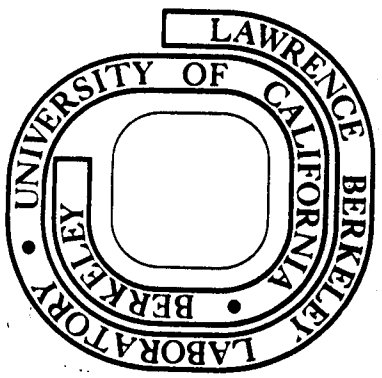

LBL-3811
c.1

DISCLAIMER

NUCLEAR INSTRUMENTS AND METHODS 122 (1974) 575–585; © NORTH-HOLLAND PUBLISHING CO.

A BREMSSTRAHLUNG-IDENTIFICATION TECHNIQUE FOR COSMIC-RAY ELECTRONS AND POSITRONS

ANDREW BUFFINGTON, CHARLES D. ORTH and GEORGE F. SMOOT

Space Sciences Laboratory and Lawrence Berkeley Laboratory, University of California, Berkeley, California 94720, U.S.A.

Received 19 September 1974

We introduce a new technique to separate energetic e^+ and e^- from a background of other particles. The technique utilizes a selective trigger, radiation of bremsstrahlung photons by incident $e^\pm$, magnetic deflection of the $e^\pm$ after photon emission, and the separate detection of both the $e^\pm$ and the photons in a shower detector. Descriptions are given of a balloon-borne apparatus using this technique for cosmic-ray $e^\pm$ spectral measurements in the energy range from 5 to 50 GeV. Calibrations of the apparatus at particle accelerators and the method of flight data analysis are also described. Our balloon-borne apparatus provides an efficiency of about 50% for the detection of $e^\pm$ and a proton rejection of about 10^{-5}.

1. Introduction

In this paper we introduce a new technique for identifying and separating energetic e^+ (positrons) and e^- (negatrons, electrons) in the primary cosmic rays while providing powerful rejection of the plentiful background of heavier particles. Many other techniques for identifying $e^\pm$ already exist. Cherenkov counters, for example, are commonly employed both at accelerators[1]) and in cosmic-ray measurements[2]). Visual examination of shower development[3]), energy measurement in a total absorption device[4]), and identification of shower development profiles[5]) have also been employed. Recently, experimenters have had success identifying $e^\pm$ through detection of transition radiation X-rays[6]). It has even been suggested that $e^\pm$ in high energy beams could be individually identified by detecting the synchrotron radiation they emit while passing through bending magnets[7]).

Some of these techniques have been used to measure primary cosmic-ray $e^\pm$ fluxes from balloons or satellites. These measurements should provide a vital probe of cosmic-ray origins and history. Unfortunately, the reported fluxes span a factor of four at 5 GeV[8]), presumably because $e^\pm$ efficiency and background rejection have often been poorly assessed. Accurate assessment of background is particularly important for e^+ measurements since cosmic-ray protons outnumber e^+ by a factor of 1000. Because of this large background and the low e^+ flux, separate e^+ measurements have been reported only below 5 GeV[9,10]). Attempts have been made to infer the e^+/e^- ratio above this energy from the east–west asymmetry in arrival direction[11,12]).

Although a single application of any of the previously used techniques provides high efficiency for $e^\pm$ identification, the rejection of strongly interacting background particles is not much greater than 10^{-3}. Placing several $e^\pm$ identification techniques in series can of course provide better background rejection. A single application of our new technique results in rejections of about 10^{-5}.

Our technique is based on the simultaneous detection both of a particle and its accompanying bremsstrahlung radiation. This radiation is characteristic of $e^\pm$ but not of heavier background particles. Although other techniques also rely on bremsstrahlung radiation through detection of the resulting electromagnetic showers, we use a magnetic field to separate the $e^\pm$ from its radiation before any further shower development has occurred. Two separate showers are then observed at the proper locations in a detector employing heavy absorbers. It is this unique signature which gives our technique its great background rejection.

We describe the basic method and theory in more detail in section 2. In sections 3 and 4 we describe a balloon-borne apparatus for the measurement of primary e^+ and e^- cosmic-ray spectra from 5 to 50 GeV. Related accelerator calibrations and the detailed methods of data analysis are also described. Efficiencies and background are investigated in sections 5 and 6. Limitations of the technique are discussed in section 7. The astrophysical results are presented elsewhere[13]).

2. Basic method and theory

Fig. 1 shows the essential features of our new "bremsstrahlung-identification" technique. An incident $e^\pm$ emits bremsstrahlung photons while passing through a thin lead radiator. A magnetic spectrometer separates the $e^\pm$ from its bremsstrahlung photons, measures its momentum, and determines the sign of its

charge. Finally the photons and $e^{\pm}$ enter a shower detector where both are observed visually. The spatial separation between the two showers and their absolute locations in the shower detector are predicted from the measurements in the magnetic spectrometer. The appearance of this characteristic two-shower signature in the shower detector permits very great rejection of other particles. The rejection is achieved at some cost in $e^{\pm}$ efficiency, however, since not all $e^{\pm}$ have bremsstrahlung photons meeting the required topological criteria. We now turn to a detailed discussion of the processes involved.

The probability that a singly charged particle of mass m and total energy E emits a bremsstrahlung photon with fractional energy fE upon passing through a radiator of thickness dx radiation length is given by[14])

$$\phi(E,f)\,df\,dx = \left(\frac{m_e}{m}\right)^2 \frac{G(E,f)}{f}\,df\,dx, \qquad (1)$$

where m_e is the rest mass of the $e^{\pm}$. For incident $e^{\pm}$ with $E \gtrsim 5$ GeV, $G(E,f)$ is independent of E except for f very close to unity[14]):

$$G(E,f)|_{e^{\pm}} = 1+(1-f)^2-\tfrac{2}{3}(1-f)+\tfrac{1}{9}(1-f)/\ln(183/Z^{\frac{1}{3}}), \qquad (2)$$

where Z is the atomic number of the radiator. For heavier spin-$\frac{1}{2}$ particles (e.g. protons) and for spin-0 particles (pions), $G(E,f)$ is a function of E, but is comparable to or smaller than the $G(E,f)$ in eq. (2) for the energies $E>5$ GeV of interest here.

Bremsstrahlung radiation is therefore characteristic of $e^{\pm}$ but not of heavier particles because of the $(m_e/m)^2$ factor in eq. (1). This factor is 10^{-4} for muons and 3×10^{-7} for protons. This inhibited bremsstrahlung photon emission is what suggested to us that energetic $e^{\pm}$ could be uniquely identified, even in a large background of heavier particles, by simultaneously detecting both the $e^{\pm}$ and at least one accompanying bremsstrahlung photon.

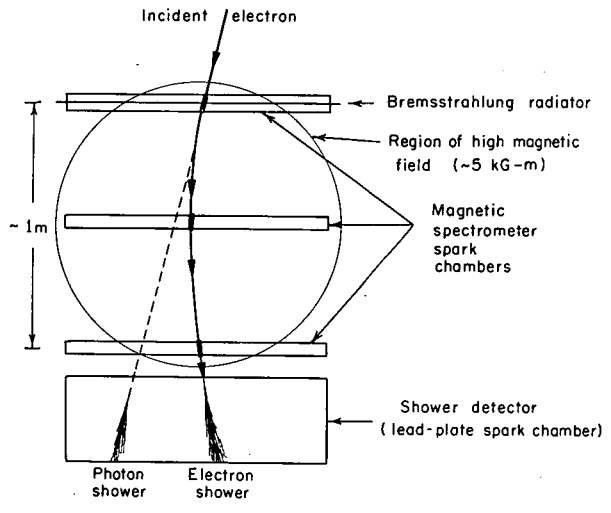

Fig. 1. Schematic diagram for the technique.

Bremsstrahlung photons are emitted at a mean angle

$$\theta_{rms} \approx \frac{q\ln\gamma}{\gamma}, \qquad (3)$$

where $\gamma = E/m_e c^2$ and q is a quantity of order unity which depends weakly upon f and Z. For energies above 4 GeV, θ_{rms} is always less than a milliradian. As a result the two trajectories are very close together and separate detection of an $e^{\pm}$ and its photons is ordinarily extremely difficult. We made the separate detection easier by using a magnetic field to deflect the $e^{\pm}$ but not the photons.

The ideal thickness ΔX of the radiator depends on the desired efficiency for $e^{\pm}$ detection and on the minimum photon energy E'_{min} that can be detected. If we take the photon detector to be infinitely thick, we can neglect leakage out the rear and the mean number of detected photons will simply be the number N of photons radiated with energy $E'>E'_{min}=f_{min}E$:

$$\begin{aligned} N(f_{min}) &= \int_0^{\Delta X} dx \int_{f_{min}}^1 df\,\phi(E,f) \\ &= \Delta X\{\tfrac{4}{3}[-\ln f_{min}-(1-f_{min})+\tfrac{3}{8}(1-f_{min}^2)] \\ &\quad +\tfrac{1}{9}[-\ln f_{min}-(1-f_{min})]/\ln(183/Z^{\frac{1}{3}})\}. \end{aligned} \qquad (4)$$

This result ignores the small degradation of E and hence the changing value of f_{min} which would occur in passing through a finite thickness ΔX of radiator. For rough calculations, one may use the approximate relation $N\approx1.3$ photons radiated per radiation length per natural logarithmic interval in E.

The efficiency ε for identifying $e^{\pm}$ with such an infinitely thick detector is given simply by:

$$\varepsilon = 1-\exp[-N(f_{min})]. \qquad (5)$$

For 90% efficiency, $N(f_{min})$ must be about 2. This implies that a thickness ΔX of about $\frac{1}{4}$ radiation length yields $N(f_{min})=2$ for $f_{min}=10^{-3}$.

In practice, the shower detector cannot be infinitely thick so some bremsstrahlung photons are lost out the rear. There are other processes which also contribute to a loss of $e^{\pm}$ events, such as the interaction of bremsstrahlung photons before they leave the radiator.

Proper evaluation of $e^{\pm}$ efficiency therefore requires a detailed analysis of the particular apparatus used.

The radiator degrades the energy of an $e^{\pm}$ in producing bremsstrahlung photons. By definition the average energy degradation is just $e^{-\Delta X}$ for a given incident energy E and a radiator of thickness ΔX radiation lengths. On the other hand, if we ask from what E on the average did a given degraded energy E^* arise, we must resort to an analysis dependent on the incident spectrum. Consider, for example, the incident power-law spectrum

$$\frac{dN(E)}{dE} = AE^{-j}, \tag{6}$$

and the quantities

$$Q_n(E^*) = \int_{E^*}^{\infty} dE \frac{dN(E)}{dE} P(E, E^*, \Delta X) \left(\frac{E^*}{E}\right)^n, \tag{7}$$

where $P(E, E^*, \Delta X)$ is the probability for degradation in the radiator from primary energy E to within dE^* of energy E^*. Using eq. (6) and $P(E, E^*, \Delta X) \approx \approx \{(\ln (E/E^*))^{(\Delta X/\ln 2)-1}/\Gamma(\Delta X/\ln 2)\}/E$, where Γ is the gamma function[15]), we obtain

$$Q_n(E^*) = A(j+n)^{-\Delta X/\ln 2}(E^*)^{-j}. \tag{8}$$

If we now choose a given E^* and ask what the average energy degradation is for events producing an $e^{\pm}$ at (or above) E^*, the answer is

$$\langle E^*/E \rangle = Q_1/Q_0 = [(j+1)/j]^{-\Delta X/\ln 2}, \tag{9}$$

Moreover, the average scaling factor required to shift the degraded energies for these events to their respective incident energies is

$$\langle E/E^* \rangle = Q_{-1}/Q_0 = [(j-1)/j]^{-\Delta X/\ln 2}. \tag{10}$$

Eqs. (9) and (10) are not precise because they are based on the above approximation for $P(E, E^*, \Delta X)$. Monte Carlo calculations indicate, however, that eqs. (9) and (10) are respectively low and high by only about 3.5% per radiation length, a negligible error for our purposes.

Note that an incident spectrum given by eq. (6) is degraded on passing through a radiator to $Q_0(E^*)$:

$$\frac{dN(E^*)}{dE^*} = Q_0(E^*) = A'(E^*)^{-j}, \tag{11}$$

$$A' \approx A(j^{-\Delta X/\ln 2}). \tag{12}$$

By comparing eqs. (11) and (6), we see that the bremsstrahlung process leaves the spectral index j unchanged. This result has already been noted by Schmidt[16]) using the approximation for $P(E, E^*, \Delta X)$ mentioned above, but follows to better approximation merely from the absence in eq. (2) of any explicit mention of the $e^{\pm}$ energy E.

Very great background rejection for our technique arises from the unique double-shower signature. The small value for θ_{rms} means that the photon shower occurs at an accurately predictable place in the shower detector. To utilize this fact, it is imperative that the magnetic spectrometer include spatial detectors which can determine the precise trajectory of the $e^{\pm}$ after its bremsstrahlung emission. The $e^{\pm}$ shower must occur along this trajectory where it enters the shower detector, while the bremsstrahlung photon shower must occur along the tangent defined where the trajectory passes through the radiator. It is a comparison of the observed shower locations with these expected locations which provides the final background rejection.

For practical application, to reduce the number of unwanted background events recorded, a selective trigger may be employed. This trigger can require that a single particle traverse the spectrometer and then deposit a large amount of energy in a scintillator placed behind several radiation lengths of heavy absorber. Since such a trigger accepts only those events in which significant interaction occurs in the absorber, it thereby eliminates practically all of the muons incident, and a large fraction of the pions and protons. If the absorber thickness and scintillator threshold are properly chosen, this initial background rejection occurs without significant loss of $e^{\pm}$ events, since these are characterized by a large shower in the absorber. For example, with an absorber thickness of 3 radiation lengths and $e^{\pm}$ energies from 5 to 50 GeV, we have found (both by computer simulation and by experience) that a threshold of about 11 times minimum ionization in the scintillator provides typically 80% rejection against protons, but still accepts over 97% of $e^{\pm}$.

3. Apparatus

Fig. 2 shows a diagram of the apparatus used for our cosmic-ray $e^{\pm}$ studies and table 1 gives a list of its specifications[17]). The superconducting magnetic spectrometer is very similar to our first-generation instrument[18]), but features improved magnet, cryogenics, and optics. The bremsstrahlung radiator had a total thickness of 0.32 radiation length and was placed between the two modules of the spectrometer top spark chamber. Each optically viewed spectrometer spark chamber had four gaps and had a spatial resolution of 0.1 mm. A 24-gap lead-plate spark chamber placed below the spectrometer served as the shower detector.

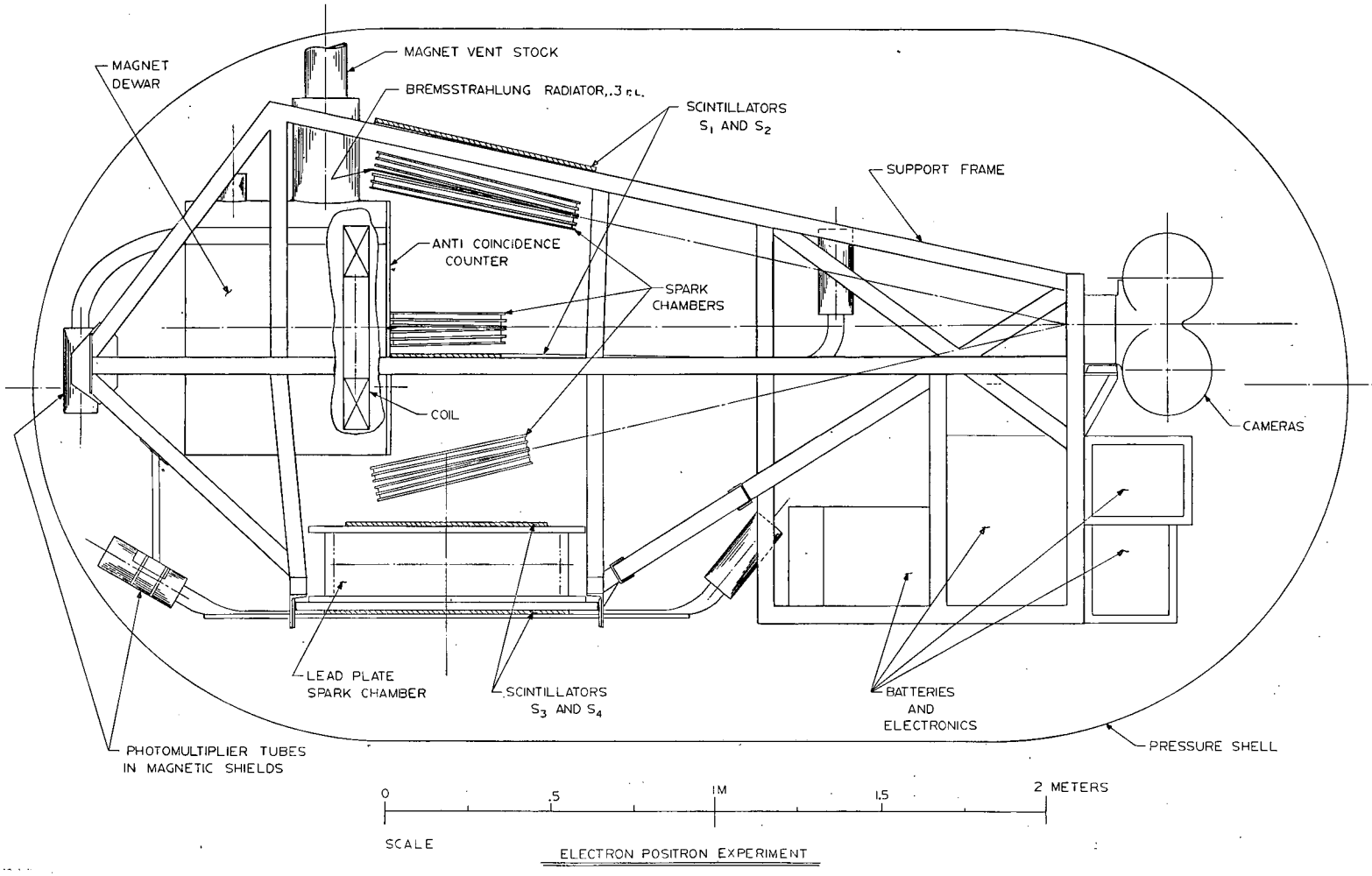

Fig. 2. Schematic diagram for the balloon flight apparatus. The figure shows the outer pressure shell, main frame, electronics locations, and detector layout.

TABLE 1

Specifications of the balloon flight apparatus.

Pressure shell (fiberglass glued to aluminium flange)		
	length	4.0 m
	diameter	2.1 m
Gondola	weight	1800 kg
Magnet coil	inner radius	17.5 cm
	outer radius	31.7 cm
	width	8.0 cm
	turns	14 886
	material	Ni-Ti, Cu-clad
	filaments	180
	copper to superconducting ratio	1.8:1
	maximum operational current	117 A
	apparent current density	14 600 A/cm^2
	average magnetic field integral (110 A)	5.1 kG m
Trigger scintillators (all are Pilot Y, 1 cm thick)		S_1 69 cm × 89 cm S_2 33 cm × 75 cm S_3 61 cm × 81 cm S_4 71 cm × 76 cm
Geometry factor		(0.084 ± 0.003) m^2 sr
	scattering material within spectrometer	1.4 g/cm^2 0.04 radiation lengths
	spark chamber gap spacing	1.5 cm in each of 4 gaps/chamber
	spark reconstruction accuracy	0.1 mm/spark chamber
	Resulting specific curvature accuracy (for $Z = 1$)	(80 GV/c)$^{-1}$
Bremsstrahlung radiator	lead	0.32 radiation lengths
	other gondola material above spectrometer	0.07 radiation lengths
Lead-plate spark chamber		
	Active area	69 × 74 cm
	gap spacing	0.5 cm
	6 aluminum plate gaps	0.02 radiation lengths each
	18 lead gaps	0.16 radiation lengths each

The first six plates of this chamber were constructed of 0.04 radiation length aluminum to delay photon conversion and thus aid in the rejection of multiprong background (i.e. multiple charged-particle entry). The other plates were 0.16 radiation length lead, and the total thickness of the chamber was about 3 radiation lengths. Four trigger scintillators were used, three in the spectrometer, and one below the lead-plate chamber.

We calibrated the lead-plate chamber at accelerators to verify the feasibility of the basic technique and to measure the rejection and acceptance efficiencies to be described in sections 5 and 6. The chamber was then assembled with our magnetic spectrometer in a gondola for balloon flight and flown to an altitude of about 35 km. Particles meeting our trigger scheme had to traverse the first three scintillators and then deposit at least 11 times minimum ionization in the bottom scintillator. For most of the flight, we also required that there be no count in an anti-coincidence scintillator and no greater than 2.5 times minimum ionization response in the first scintillator. About 10% of the data were recorded without the anticoincidence scintillator included in the trigger, but operating a light photographed with the spark chambers. Out of 69 good events in this sample, only one would have been vetoed by the anticoincidence scintillator. This puts the loss of data due to the anticoincidence scintillator at about 2%. The loss of data due to the 2.5 times minimum-ionizing upper bound on the first scintillator is expected to have been even smaller.

Figs. 3 and 4 show respectively an e^+ event and a proton event from the flight. These pictures clearly show how the bremsstrahlung-identification technique achieves its great rejection against proton events.

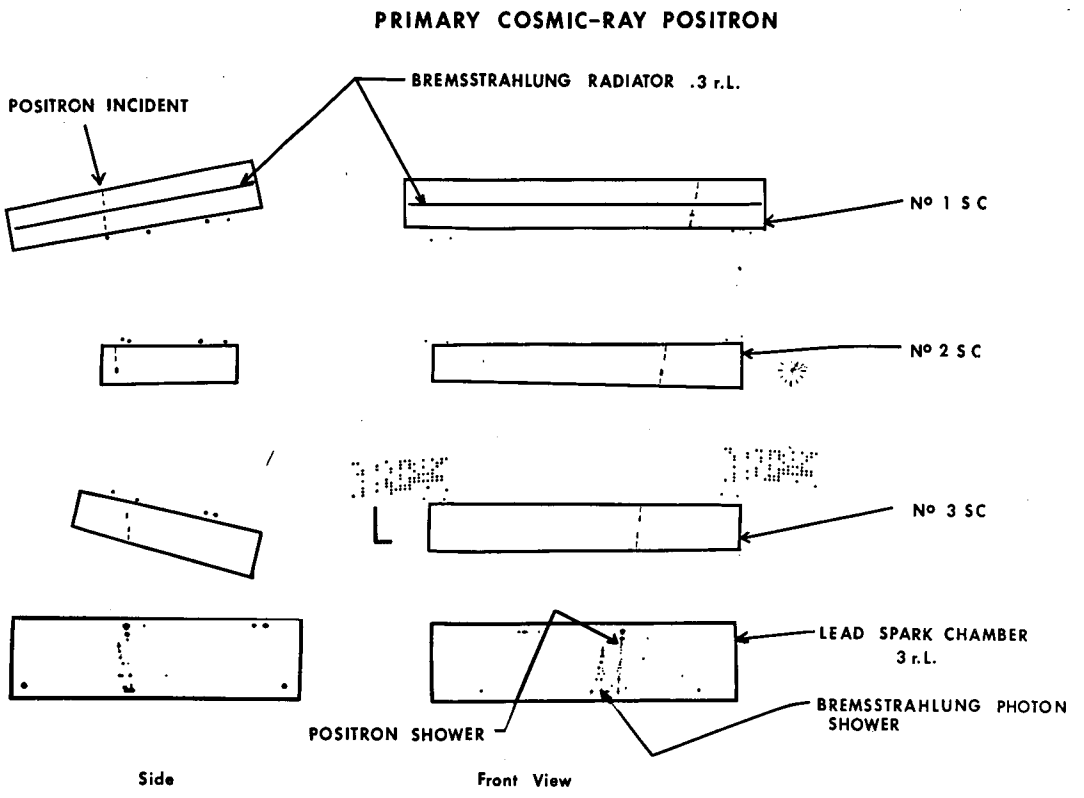

Fig. 3. Cosmic-ray positron recorded in the apparatus. The spark chamber format has been re-arranged here and in fig. 4, to put both front and side views of the sparks in the correct spatial relationship. Measured energy is about 5 GeV.

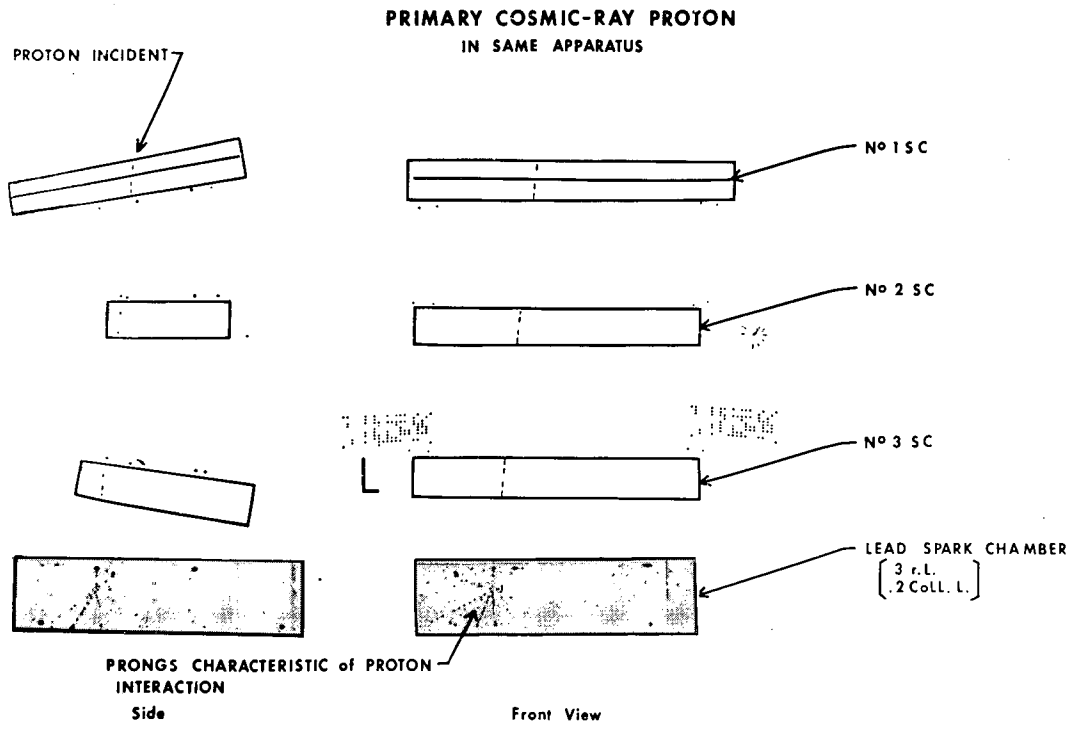

Fig. 4. Cosmic-ray proton recorded in the apparatus.

4. Data analysis

Film from the flight was scanned using the following criteria for acceptable $e^{\pm}$:

1) In the lead-plate chamber
(a) only one charged particle incident from above;
(b) no obvious prongs (like those of fig. 4);
(c) at least one photon conversion.

2) In the momentum spectrometer
(a) a single trajectory passing through all three chambers;
(b) no more than one extra track visible in the chambers.

A prong in the lead-plate chamber was defined as a roughly co-linear sequence of at least 5 sparks pointing back towards the charged particle trajectory. Bremsstrahlung showers were also required to have sparks in at least 5 gaps but to be approximately parallel to the incident trajectory. This 5-gap criterion limited the lead-plate chamber to photons of energy greater than $E'_{min} \approx 10$ MeV, and to a fiducial volume of total thickness 2.15 radiation lengths since no bremsstrahlung shower could begin after gap 20.

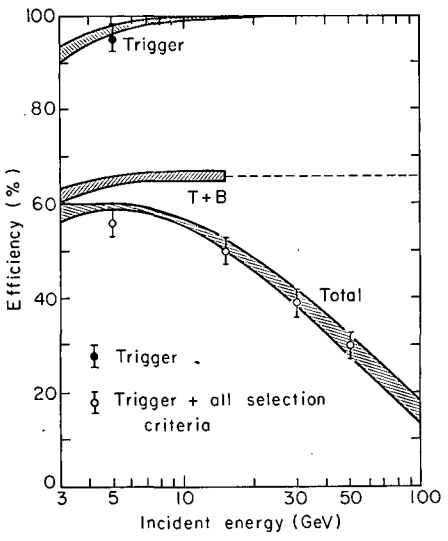

Fig. 5. Triggering and identification efficiency, as measured at SLAC. The hatched curves indicate expected values, as calculated by our Monte Carlo program. Top curve (Trigger): trigger efficiency alone. Middle curve (T+B): expected efficiency for events meeting all bremsstrahlung identification criteria; dashed portion indicates efficiency for simulated higher energy runs. Bottom curve (TOTAL): expected efficiency, when the effects of track merging in the lead-plate spark chamber have been taken into account. The higher momenta (30 and 50 GeV/c points) were simulated at SLAC by reducing the current in the spectrometer magnet.

About 20% of the protons incident downward on the apparatus in flight met the trigger criterion. About 25% more triggers were caused by interactions of wide-angle particles above the lead-plate chamber. To eliminate the latter, we rejected any $e^{\pm}$ event whose photon conversions started before gap 3 of the lead-plate chamber. Such conversions could occur within the bremsstrahlung radiator, in the spectrometer, or in the first two gaps of the lead-plate chamber. Our chosen radiator thickness was a compromise between too few bremsstrahlung photons to get a good identification efficiency, and so many that conversions before the third gap of the lead chamber would cause excessive rejection of the data.

For flight data, typically one event in thirty satisfied the above selection criteria. These were 10^{-2} of the background events, and about half of the $e^{\pm}$ events. All of the data were double scanned, and nearly half of the data triple scanned, for a total scanning efficiency of 99%.

After the events were selected, their trajectories and shower locations were measured, and our computer program determined the sign of the particle's charge, its momentum, and the expected locations for the $e^{\pm}$ and photon showers in the lead chamber[19]). Two-thirds of the background events failed to have a good fit. The expected double shower locations were then compared with the observed locations on an event-by-event basis. Any event whose bremsstrahlung shower was mislocated by more than 1 cm and by more than 30% of the double-shower spacing was rejected as background. This final requirement gave at least forty times more rejection against the background.

5. $e^{\pm}$ acceptance efficiency

To determine the $e^{\pm}$ efficiency of the apparatus we exposed the lead-plate chamber and bremsstrahlung radiator (without the momentum spectrometer and 0.07 radiation length of gondola material) to 5 and to 15 GeV e^- beams at the Stanford Linear Accelerator Center (SLAC). For these calibrations a bending magnet was located between the bremsstrahlung radiator and the lead chamber. Its current was set to simulate the average bend of the flight magnetic spectrometer. Two additional sets of data were taken with the current in this magnet reduced to bring bremsstrahlung and e^- showers closer together and thereby simulate 30 and 50 GeV incident e^-. Since early shower development depends only logarithmically on the incident $e^{\pm}$ energy, these data provided a good approximation to the way real higher energy events would appear in the apparatus.

The e^- events recorded at SLAC were scanned for e^--like topologies to determine the efficiency of the bremsstrahlung-identification technique for the various energies recorded. The data points in fig. 5 show the resulting measured efficiencies as a function of incident energy. Most of the e^- events without the double-shower topology were ones in which either no photon conversion showed within the fiducial volume of the lead-plate chamber or a photon converted before the third gap of the lead-plate chamber and caused the event to appear as two or more incoming particles.

The drop in efficiency at high energies in fig. 5 is qualitatively what we expect from a phenomenon called track merging. Track merging can be described as follows. When two tracks in our spark chamber are close together, typically within a millimeter, the sparks merge, appearing on the photographic record as a single track. When the energy of the incident $e^\pm$ is high enough, a bremsstrahlung photon and a degraded $e^\pm$ are not sufficiently separated by the magnetic field to appear as two independent showers. Thus, for our spark chamber, track merging sets an upper limit to the incident energy for which the bremsstrahlung-identification technique is useful. The gradual fall-off in efficiency which sets this limit is a direct result of fluctuations in the depth at which photon conversion occurs in the chamber, fluctuations in the lateral development of an $e^\pm$ shower with increasing depth, and variations in $e^\pm$–photon separations.

To determine what part of the observed drop in efficiency in fig. 5 was due to track merging, we constructed a Monte Carlo computer program to simulate the bremsstrahlung radiation and detection process for our apparatus. It calculated bremsstrahlung radiation according to eqs. (1) and (2) with the known radiation lengths of material in our apparatus, and photon conversions according to the standard cross-sections[20]) for photon energies greater than $E'_{\min} = 10$ MeV. Various photon loss mechanisms were considered: photon conversion in the radiator; conversion in the lead chamber prior to the third gap; no photon conversion above 10 MeV in the lead chamber; and bremsstrahlung involving such large energy transfer to the photon that the degraded $e^\pm$ was enough deflected by the magnet to miss the lead chamber. These loss mechanisms were responsible, respectively, for 10%, 10%, 20% and 2% loss of incident $e^\pm$ events. Triggering efficiency was also inserted as a function of incident energy according to the predictions of another computer program[21]).

The departure of the observed data from the efficiency predicted using the above Monte Carlo program was ascribed to track merging even though other effects might contribute. To parametrize the departure we selected the following simple function

$$\text{Probability of merging} = \exp\left[-a/(d-b)\right], \quad (13)$$

where d is the distance in the lead-plate chamber between the $e^\pm$ and the bremsstrahlung photon trajectories (proportional to $1/E^*$ of the degraded $e^\pm$). Fixed constants a and b are presumably determined by the detailed construction and powering scheme of the lead-plate chamber. A fit to the data gave $a=(1.4\pm\ \pm 0.2)$ mm and $b=(0.3\pm 0.3)$ mm. Fig. 5 presents the results of the Monte Carlo calculations (hatched curves). The bottom curve includes the effects of track merging.

As shown in fig. 5, the expected efficiency as a function of energy ignoring track merging was approximately constant at SLAC except for triggering efficiency. The constancy above 15 GeV reflects the assumption that higher energy points were really 15 GeV points with reduced magnetic fields. The merging was therefore the only contributer to the drop in efficiency observed for the simulated high energies at SLAC.

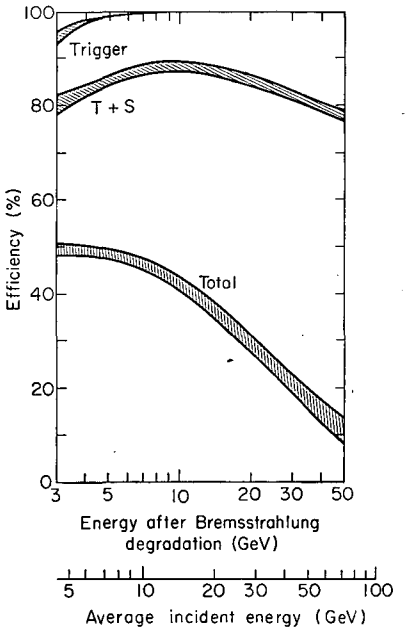

Fig. 6. Expected efficiencies for the flight apparatus. Top curve (T): trigger efficiency alone. Middle curve (T+S): events satisfying both trigger and spectrometer criteria, the proper efficiency curve for e^-. Bottom curve (TOTAL): events satisfying all bremsstrahlung-identification criteria, the proper efficiency curve for e^+. The lower energy scale indicates the average incident energy at the top of the atmosphere, for a spectral index of $j = 2.8$.

We made a cross-check to verify the validity of the track-merging prescription in the slightly different geometry used in flight. This was done by making a separate scan of flight data to select negatively charged events which showered in the lead chamber and satisfied all scanning criteria except that a bremsstrahlung conversion [1(c) of section 4] was not required. Since a negligible number of muons and few pions can meet our trigger and prongless criteria, the 673 negatively charged events thus found were presumably almost exclusively e^-. $58 \pm 3\%$ of these had identifiable bremsstrahlung conversions. This compares favorably with the Monte Carlo prediction of 59%.

Fig. 6 presents the Monte Carlo efficiency calculations for the flight geometry as a function of degraded energy measured by the spectrometer. The widths of the hatched curves indicate the possible errors in the predictions. The e^- events described in the preceding paragraph are displayed in fig. 7 as a function of degraded energy through the measured ratio for e^-:

$$R = \frac{\text{events satisfying all bremsstrahlung-identification criteria}}{\text{events satisfying trigger and spectrometer topology criteria}}$$

The associated Monte Carlo prediction is also shown. Again, the agreement between prediction and observation is good, thereby providing a flight cross-check of the curves in fig. 6.

Since negative-charged background in the primary cosmic rays is low, we regard the middle curve of fig.6 as the proper efficiency for e^-. This applies only to e^- selected on the basis of good topology in the spectrometer and prongless showers in the lead-plate chamber. However, because of the large proton background, we require the full bremsstrahlung identification for e^+

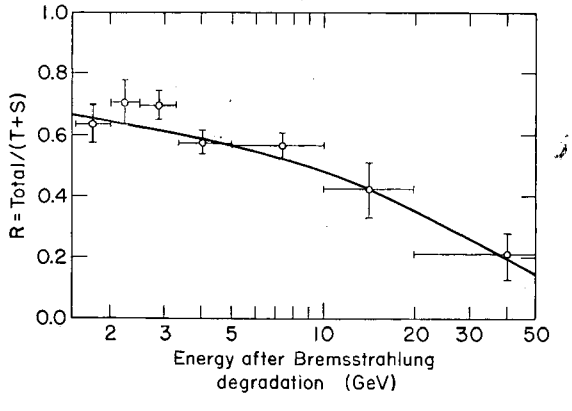

Fig. 7. Flight data cross-check of the ratio R of curves TOTAL/(T+S) in fig. 6, using the background-free e^- data sample.

(bottom efficiency curve). Our average efficiency for e^- is $77 \pm 2\%$, and our average efficiency for e^+ is $46 \pm 2\%$.

We have included an incident-energy scale in fig. 6. This is based on the assumed scaling ratio of 1.4 obtained from eq.(10) for an incident $e^\pm$ spectral index of $j = 2.8$ and our flight value of $\Delta X = 0.54$. This scaling ratio typically decreases by 0.05 as j is increased by 0.2. Such fixed power-law behavior is altered by geomagnetic cutoff effects, which cause rapid departure from the power-law dependence. For our flight data with a mean 4 GV/c cutoff, fixed scaling cannot be used for $E^* \lesssim 5$ GeV.

6. Background

In order to measure the background from protons directly, we exposed the basic apparatus to 1.5×10^5 protons of 4.5 GeV/c from the Lawrence Berkeley Laboratory Bevatron. 1.1×10^4 events met the trigger criterion and were photographed. A double scan of these events disclosed 23 with bremsstrahlung-photon-like shower activity in the lead chamber. No more than one or two of these events could possibly have had showers properly located to be identified as true $e^\pm$ events. This calibration therefore established the technique's rejection against protons to be about 10^{-5} at 4.5 GeV/c.

To obtain the final measure of background rejection for our flight data, we plotted the differences between the predicted and the observed locations of the bremsstrahlung showers in the lead chamber. Fig. 8 shows the results for our data. The spread of points on the plot, due mostly to multiple Coulomb scattering in the bremsstrahlung radiator, is about 4 mm. Also shown are the projected distributions expected on the basis of Monte Carlo calculations. Some background contamination in the form of showers occurring in the wrong places is apparently present. If all the events outside the box in fig. 8 form a smooth background, we would conclude that no more than one or two events from proton interactions could be expected to lie within the selection box shown. This is consistent with the ≈ 1 event that we would expect from the Bevatron calibration. Since there are several hundred events inside the selection box, background contamination must indeed be negligibly small, even for our e^+ sample.

The above measurements are consistent with an order-of-magnitude calculation using particle interaction properties. We have already seen how the factor $(m_e/m)^2$ in eq.(1) makes direct bremsstrahlung radiation negligibly small for heavy particles. A proton or other hadron could undergo a nuclear interaction in the radiator or subsequent apparatus, producing

one or more neutral pions which then decay into photons. However, for this to satisfy our requirements, no extra charged prongs can appear in the spectrometer, and one of the photons must travel in the right direction to within a few milliradians. We can estimate the probability for this neutral-pion contribution by computing the average angle θ characteristic of secondary particles leaving a high-energy interaction:

$$\theta \approx \frac{(0.3\ \text{GeV}/c\ \text{transverse momentum})}{(\text{inelasticity} * \text{incident energy/multiplicity})}. \quad (14)$$

If the incident proton has energy from 10 to 100 GeV, the multiplicity is roughly 4 produced particles. The inelasticitity in such interactions is generally 0.5, thus giving pion emission angles of typically 100 milliradians. The decay of neutral pions into photons increases this typical angle. The chance that a photon lies within the proper 20 mrad square bin is therefore several percent, with the probability increasing with increasing energy. The chance of a proton interacting in the radiator in the first place is about 0.01. The chance of no charged prongs in the spectrometer is perhaps 0.2. Combining these factors, we expect a rejection between 10^{-4} and 10^{-5} over our range, as we have observed.

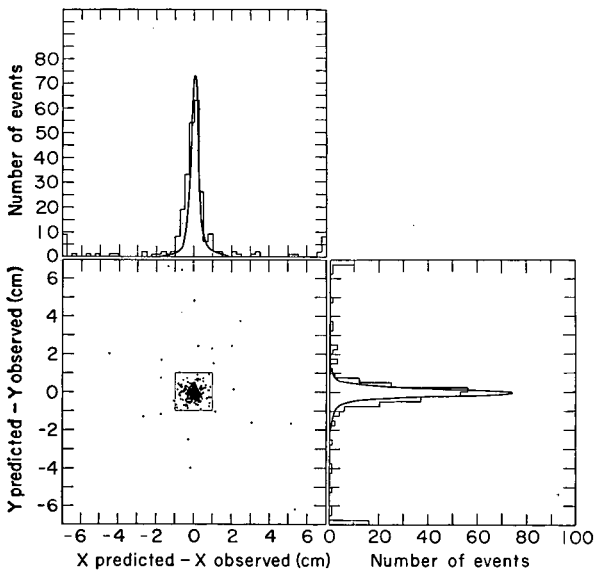

Fig. 8. Comparison of bremsstrahlung photon real space location as predicted by the spectrometer measurement, and as actually observed for a portion of our $e^{\pm}$ data. We have included events only above 2 GeV in the spectrometer, since multiple Coulomb scattering broadens the distribution below this energy. Events outside of the 2 cm box are rejected as "background" even though five of them apparently have negative charge. The last bins on the projection histograms include events off scale.

7. Discussion

The previous section shows that the bremsstrahlung-identification technique is capable of very great rejection against particles other than $e^{\pm}$. The selection efficiency for $e^{\pm}$ is very dependent on the particular choice of shower detector. The spark-chamber technique we have used has an average efficiency of 46% and our particular apparatus is limited to $e^{\pm}$ with energies less than about 50 GeV. This high-energy limit is not fundamental to the technique and could be raised by increasing the bending power of the magnet or the drift space between magnet and shower detector. It could also be increased by using a shower detector with much finer spatial resolution for detecting photon showers very close to the $e^{\pm}$ track.

The bremsstrahlung-identification technique could conceivably be valuable in a particle physics experiment where $e^{\pm}$ must be separated from a large background of other particles. Many particle physics experiments, however, would find the energy degradation a serious detriment. This limitation could be overcome by following the shower detector with a total absorption device to measure residual shower energy, and designing the shower detector itself to measure or at least sample energy. On the other hand, a shower detector could be employed which has a much smaller least detectable photon energy E'_{min} than the lead-plate chamber we used. The thickness ΔX of the bremsstrahlung radiator could then be diminished without harm to the overall efficiency, thereby decreasing the amount of energy degradation suffered by the $e^{\pm}$ upon passing through the radiator.

We would like the thank Prof. D. H. Frisch at the Laboratory for Nuclear Science, M.I.T., for the loan of the lead-plate spark chamber used in this work. The accelerator tests, vital to the successful application of this technique, would have been impossible without the assistance of the Bevatron staff, and of Dr R. Gearhart and the operations personnel at SLAC. We are grateful for the fine service and hospitality offered us by the staff of the National Center for Atmospheric Research Balloon Facility at Palestine, Texas. Numerous ideas and much support for this work came from the other members of this group, particularly L. H. Smith and R. A. Muller. W. Mountanos helped with the early accelerator tests of this technique. It is a pleasure to acknowledge the continual encouragement of L. W. Alvarez. This work was supported by N.A.S.A. contract no. NAS 9-7801 and by the Lawrence Berkeley Laboratory.

References

1) J. Litt and R. Meunier, Ann. Rev. Nucl. Sci. **23** (1973) 1.
2) D. Hovestadt, P. Meyer and P. J. Schmidt, Nucl. Instr. and Meth. **85** (1970) 93.
3) B. Agrinier et al., Nucl. Instr. and Meth. **88** (1970) 109.
4) R. Hofstadter, Science **164** (1969) 1471.
5) R. F. Silverberg et al., 12th Intern. Conf. on *Cosmic rays*, Hobart (1971) vol. 1, p. 122; and D. Müller, Phys. Rev. **D5** (1972) 2677.
6) A. I. Alikhanian, K. A. Ispirian, A. G. Oganessian and A. G. Tamanian, Nucl. Instr. and Meth. **89** (1970) 147; also M. L. Cherry, D. Müller and T. A. Prince, Nucl. Instr. and Meth. **115** (1974) 141.
7) W. Busza, M. Chen and D. Luckey, Nucl. Instr. and Meth. **105** (1972) 613.
8) W. R. Webber, 13th Intern. Conf. on *Cosmic rays*, Denver, Colo. (1973) vol. 5, p. 3568.
9) J. L. Fanselow, R. C. Hartman, R. H. Hildebrand and P. Meyer, Astrophys. J. **158** (1969) 771.
10) J. K. Daugherty, Goddard Space Flight Center Report No. X-660-74-16 (January 1974) to be published.
11) B. Agrinier et al., Lettre al Nuovo Cimento **1** (1969) 53.
12) K. C. Anand, R. R. Daniel and S. A. Stephens, 11th Intern. Conf. on *Cosmic rays* Budapest, Hungary (1969) vol. 1, p. 235.
13) A. Buffington, C. D. Orth and G. F. Smoot, Phys. Rev. Letters **34** (1974) 38; more detailed articles will be submitted to Astrophys. J.
14) For a review of electromagnetic interactions, see sections 2-11 through 2-13, B. Rossi, *High energy particles* (Prentice-Hall, Englewood Cliffs, New Jersey, 1952).
15) Op. cit., pp. 60 and 244.
16) P. J. Schmidt, J. Geophys. Res. **77** (1972) 3295.
17) A preliminary report of this work was given at the Denver Cosmic Ray Conference: A. Buffington, G. F. Smoot, L. H. Smith and C. D. Orth, 13th Intern. Conf. on *Cosmic rays*, Denver, Colo. (1973) vol. 1, p. 318.
18) L. H. Smith, A. Buffington, M. A. Wahlig and P. Dauber, Rev. Sci. Instr. **43** (1972) 1.
19) We have previously described our momentum analysis procedure in considerable detail: L. H. Smith, A. Buffington, G. F. Smoot, L. W. Alvarez and M. A. Wahlig, Astrophys. J. **180** (1973) 987.
20) Ref. 14. section 2-19.
21) C. D. Orth and A. Buffington, to be submitted to Astrophys. J.

TECHNICAL INFORMATION DIVISION
LAWRENCE BERKELEY LABORATORY
UNIVERSITY OF CALIFORNIA
BERKELEY, CALIFORNIA 94720